ELSEVIER

Journal of Organometallic Chemistry 503 (1995) 243–250

Journal of Organometallic Chemistry

Electrochemical, spectroscopic and theoretical studies of a series of 1,1′-ferrocene dichalcogenido-complexes of rhodium and iridium

Piero Zanello [a,*], Maurizio Casarin [b,*], Luca Pardi [c], Max Herberhold [d,*], Guo-Xin Jin [d]

[a] *Dipartimento di Chimica dell'Università, Pian dei Mantellini, 44, 53100 Siena, Italy*
[b] *Dipartimento di Chimica Inorganica, Metallorganica ed Analitica dell'Università, Via Loredan 4, 35131 Padova, Italy*
[c] *Dipartimento di Chimica dell'Università, Via Maragliano 77, 50144 Firenze, Italy*
[d] *Laboratorium für Anorganische Chemie der Universität, Postfach 10 12 51, D-95440 Bayreuth, Germany*

Received 6 February 1995

Abstract

The electrochemical behaviour of a series of heterodimetallic 2-metalla-1,3-dichalcogena-[3]ferrocenophanes of general formula $Cp^*(L)M[(EC_5H_4)_2Fe]$ (E = S, Se or Te; M = Rh, L = PMe_3; M = Ir, L = PMe_3, PPh_3 or $C{\equiv}N^tBu$) has been investigated. These complexes undergo two successive oxidation steps. In spite of the fact that both metal centres are potentially able to lose electrons, EPR spectra and theoretical considerations suggest that the bridging chalcogen atoms, which are centres of high electron density, also contribute significantly to the electron-removal processes.

Keywords: [3]Ferrocenophanes; Electrochemistry; EPR Spectroscopy; Theoretical calculations; Rhodium; Iridium

1. Introduction

Heterodimetal assemblies obtained by linking redox-active ferrocene units to transition metal complex fragments are gaining interest in that reversible electron-transfer processes at the ferrocene moiety may affect the adjacent transition metal centres, although leaving intact the original coordination sphere [1,2]. The most common case is that in which a ferrocene-containing ligand is bound to a transition metal complex fragment [3–8], but cases in which either two ferrocenyl-derived ligands are attached to one metal complex fragment [1,6], or ferrocenyl-type ligands are connected with metal cluster assemblies [9–15] are also known. In many of these systems, the only redox-active moiety is the ferrocene component. Exceptions are the copper(II) complexes [1] and the tricobalt clusters [10–14], which contain two redox-active centres within the molecule.

We have recently found that the metal centre of the organometallic fragment $Cp^*M(PR_3)$ in the half-sandwich complexes $[Cp^*(PR_3)M(CH_3)_2]$ (M = Rh or Ir) is able to undergo one-electron oxidation to the unusual M(IV) oxidation state [16]. We have also reported the one-electron oxidation of 1,3-trichalcogena-[3]ferrocenophanes, $Fe(C_5H_4E)_2E'$ (E,E′ = S, Se or Te) [17]. In the heterodimetal compounds considered in the present study (Scheme 1), both building blocks are combined to give 2-metalla-1,3-dichalcogena-[3]ferrocenophanes of the general formula $[Cp^*(L)M\{(EC_5H_4)_2Fe\}]$ (E = S, Se or Te; M = Rh, L = PMe_3 (**1a–c**); M = Ir, L = PMe_3 (**2a–c**), PPh_3 (**3a–c**) and $C{\equiv}N^tBu$ (**4a–c**) [18]. These complexes undergo two successive oxidation steps. At the first sight this might be attributed to a stepwise oxidation of the two metal centres. However, a theoretical study indicates that the bridging chalcogen atoms (E) are also centres of high electron density.

2. Results and discussion

The synthesis of the heterodimetal complexes in Scheme 1 and their characterisation by ^1H, ^{13}C and ^{31}P NMR spectroscopy as well as mass spectrometry has been described [18]. They are obtained easily from either $[Cp^*(L)RhCl_2]$ (L = PMe_3) or $[Cp^*(L)IrCl_2]$ (L = PMe_3, PPh_3 or $C{\equiv}N^tBu$) and the dilithium 1,1′-dichalcogenido-ferrocene, $Fe(C_5H_4ELi)_2$, in tetrahydro-

* Corresponding authors.

SSDI 0022-328X(95)05559-2

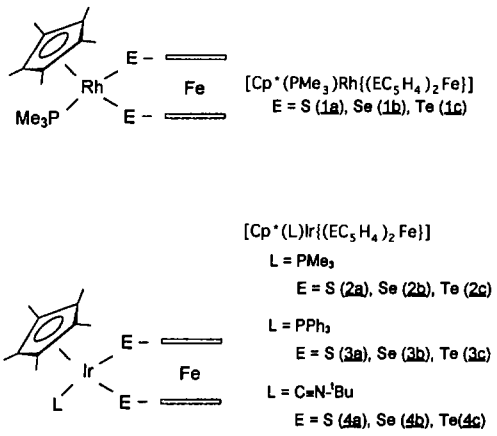

Scheme 1.

furan (THF) solution under argon. The iridium compounds are more stable than the rhodium complexes; The tellurium compounds tend to decompose slowly, both in solution and in the solid state.

Chemical oxidation using $Ag[BF_4]$ has been found [18] to lead to paramagnetic $[Cp^*(L)M\{(EC_5H_4)_2Fe\}]^+[BF_4]$, (**1b**$^+$) (violet), (**3a**$^+$) (green–brown) and (**3b**$^+$) (violet). Similar oxidations can be achieved with $Ag[PF_6]$, $Ag[SbF_6]$ and ferrocenium salts such as $[FeCp_2]^+[BF_4]$. The hexafluoroantimonate (**1b**) $[SbF_6]$ (violet) has been studied. In contrast to the tetrafluoroborate salts (**1b**) $[BF_4]$ and (**3a**) $[BF_4]$, the neutral precursors (**1b**, **3a**) are soluble in THF solution and can therefore be easily washed out.

2.1. Electrochemistry

As typical examples, the cyclic voltammetric responses shown by the triphenylphosphaneiridium compounds $[Cp^*(PPh_3)Ir\{(E\text{-}C_5H_4)_2Fe\}]$ (**3a–c**) in dichloromethane solution are presented in Fig. 1.

They undergo two successive oxidation processes at peaks A and B, respectively, which exhibit marked features of chemical reversibility, except for the ditellurido-derivative **3c**.

In all cases, controlled potential coulometric tests corresponding to the first anodic step consumed one electron/molecule.

Analysis [19] of the cyclic voltammograms of the peak-system A/D exhibited by the sulphur-bridged compound **3a** as a function of the scan rate v (varying from 0.02 to 2.00 V s^{-1}) indicates that (i) the peak current ratio ip_D/ip_A is constant and unity (ii) the peak-to-peak separation ΔEp progressively increases with the scan rate from 66 to 149 mV and (iii) the current function $ip_A v^{-1/2}$ remains essentially constant. In the same scan-rate range, the responses of peak-system B/C show that (i) ip_C/ip_B is 0.6 at the lowest scan rate, and progressively increases to unity at 1.00 V s^{-1}, (ii) ΔEp increases from 90 to 188 mV and (iii) the current function remains practically constant. All these data indicate that a simple one-electron transfer is involved in the **3a**/[**3a**]$^+$ redox change, whereas the subsequent oxidation [**3a**]$^+$/[**3a**]$^{2+}$ is complicated by chemical decomposition. The lifetime of the transient dication [**3a**]$^{2+}$ is ca. 5 s.

A similar redox behaviour is displayed by the selenium-bridged analogue **3b**. However, the ditellurium-bridged compound **3c** is apparently unable to maintain its molecular framework intact during the two successive one-electron removals, as shown by the high degree of irreversibility shown by the relevant oxidation responses. Unexpectedly, the monocation [**3c**]$^+$ is also short-lived ($t_{1/2} \approx 1$ s).

A similar trend is shown by the trimethylphosphaneiridium derivatives $[Cp^*(PMe_3)Ir\{(E\text{-}C_5H_4)_2Fe\}]$ (**2a–c**).

As for the isonitrileiridium complexes (**4a–c**), the sulphur-bridged species **4a** parallels the corresponding phosphine complexes, whereas the selenium-bridged derivative gives quite unstable mono- and di-cations. No clear data were obtained for the tellurium-bridged species.

Finally, Fig. 2 illustrates the redox behaviour of the sulphur-bridged rhodium compound **1a**, the molecular structure of which has been determined [18].

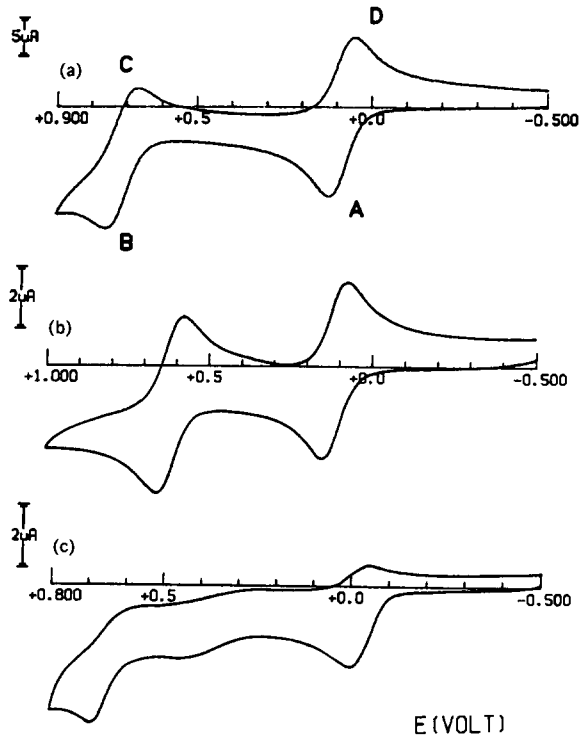

Fig. 1. Cyclic voltammograms recorded at a platinum electrode on a CH_2Cl_2 solution containing $[NBu_4][ClO_4]$ (0.2 mol dm^{-3}) and: (a) **3a** (2.1×10^{-3} mol dm^{-3}); (b) **3b** (1.0×10^{-3} mol dm^{-3}); (c) **3c** (0.9×10^{-3} mol dm^{-3}). Scan rate 0.05 V s^{-1}.

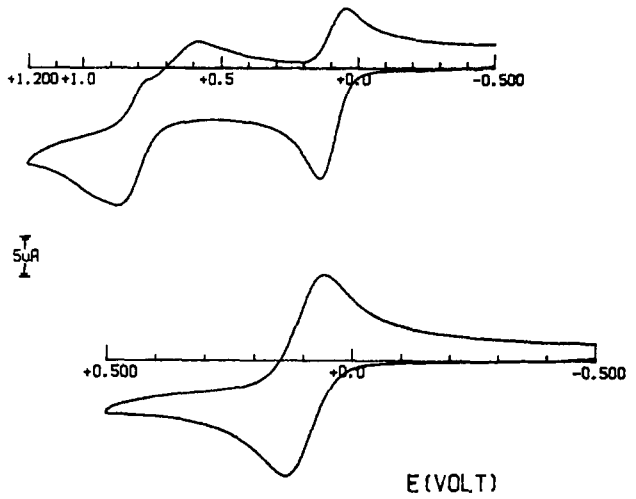

Fig. 2. Cyclic voltammograms recorded at a platinum electrode on a CH_2Cl_2 solution containing $[NBu_4][ClO_4]$ (0.2 mol dm^{-3}) and **1a** (2.1×10^{-3} mol dm^{-3}). Scan rate 0.1 V s^{-1}.

The first one-electron removal is chemically reversible, whereas the second is followed by chemical complications.

The selenium-bridged **1b** has a similar trend, but in the corresponding tellurium-bridged complex **1c** both one-electron oxidations are complicated by decomposition.

Table 1 summarizes the redox potentials for the oxidation steps exhibited by the rhoda- and irida-ferrocenophane complexes. The redox potentials for the one-electron oxidation of the mononuclear species **5–7**

Table 1
Redox potentials (in V, vs. SCE) and peak-to-peak separation (in mV) for the two successive oxidations exhibited by the heterodimetal complexes **1–4** and related compounds in CH_2Cl_2 solution

Compound	$E^{\circ\prime}(0/+)$	ΔEp [a]	$E^{\circ\prime}(+/2+)$	ΔEp [a]
1a	+0.10	68	+0.86 [a,b]	–
1b	+0.12	68	+0.68 [a,b]	–
1c	+0.03 [a,b]	–	+0.72 [a,b]	–
2a	+0.10	69	+0.74	92
2b	+0.09	71	+0.64	75
2c	0.00 [a,b]	–	+0.44 [a,b]	–
3a	+0.09	67	+0.74	92
3b	+0.12	67	+0.62	78
3c	−0.02 [a,b]	–	+0.69 [a,b]	–
4a	+0.05	81	+0.60	122
4b	+0.04 [a,b]	–	+0.56 [a,b]	–
5	+0.35 [c]	126 [c]		
6	+0.27 [c]	114 [c]		
7	+0.41	70		
8a	+0.62	72		
8b	+0.61	72		
8c	+0.57	72		
8d	+0.22	155		

[a] Measured at 0.05 V s^{-1}.
[b] Peak potential value for oxidation processes complicated by very fast decomposition.
[c] Measured at 1.0 V s^{-1} because of the relatively fast decomposition.

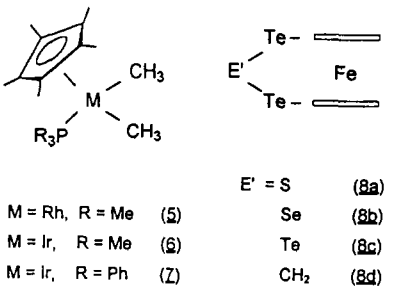

M = Rh, R = Me (5)
M = Ir, R = Me (6)
M = Ir, R = Ph (7)

E' = S (8a)
Se (8b)
Te (8c)
CH_2 (8d)

[16] and **8a–d** [17] are also reported. These mimic the two moieties of the heterodimetallic complexes **1–4** to some degree.

A naive interpretation of the data might be that, in the heterodinuclear complexes the cooperative electronic effects make the first oxidation centred on the Group 9 fragment easier and make the second oxidation centred on the ferrocene moiety more difficult, as compared with the corresponding mononuclear species. The behaviour of rhodium complexes **1a–c** and the iridium analogues **2a–c** is consistent with the reported greater lability of cationic rhodium(IV) complexes compared with the corresponding iridium(IV) species [16]. However, the results of the theoretical analysis below, indicating that both electrons are essentially removed from the bridging chalcogen atoms, do not allow such a straightforward conclusion to be drawn. In particular, if one takes into account that the first electron is removed from a chalcogen-based orbital, with contributions from both the Group 9 metal and iron, whereas the second electron is removed from a chalcogen-based orbital which contains only a contribution from the Group 9 metal, the order of the electron removal seems to be the converse.

Finally, the peak-to-peak separations in Table 1 give some insight into the structural effects accompanying the electron-transfer processes [20]. An electrochemically reversible one-electron transfer is expected to display a ΔEp value of 59 mV, independent of scan rate [19]. However, uncompensated solution resistances may affect the ΔEp value to some extent, and we are therefore justified in concluding that, in almost all cases, minimal structural changes accompany the electron transfers.

2.2. *EPR spectra of the monocations* $[Cp^*(PPh_3)Rh\{(SC_5H_4)_2Fe\}]^+$ (**[1a]$^+$**) *and* $[Cp^*(PMe_3)Ir\{(SC_5H_4)_2Fe\}]^+$ **[3a]$^+$**)

Fig. 3 shows the EPR spectra at liquid helium temperature of powdered samples of the sulphur-bridged rhodium monocation **[1a]$^+$** and the similar rhodium species **[3a]$^+$**, both obtained by macroelectrolysis as $[PF_6]^-$ salts.

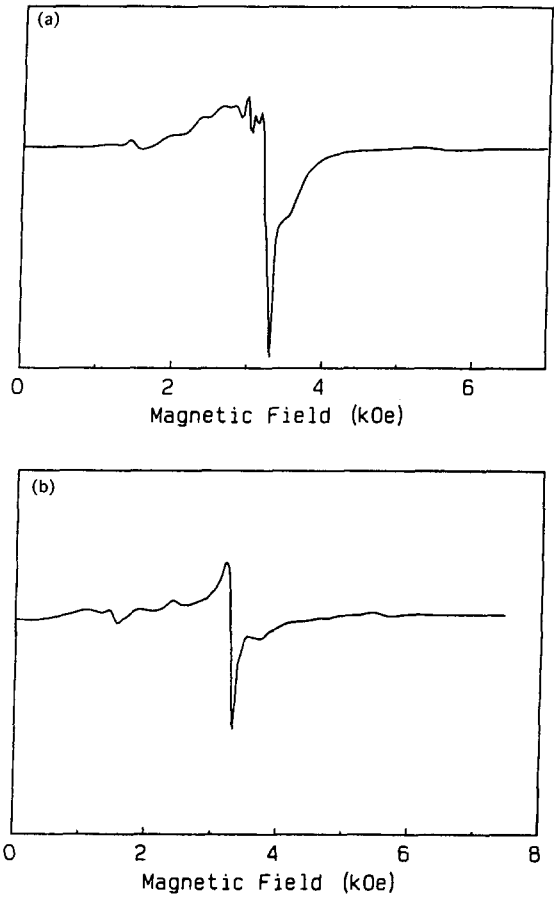

Fig. 3. X-band EPR spectra recorded at 4 K on a polycrystalline sample of: (a) **[1a]**[PF_6]; (b) **[3a]**[PF_6].

They are rather similar with an intense anisotropic peak centred at $g \approx 2$ (2.07 for $[\mathbf{1a}]^+$; 2.06 for $[\mathbf{3a}]^+$) together with several minor features in the 1000–4000 Oe range. We attribute these latter signals to impurities from decomposition. The main absorption, which is of almost the same intensity in the spectra of the two samples is quite different from that of a typical ferrocenium species [21] and resembles an organic radical, even if the linewidth (ca. hundred Oe) and the anisotropy both suggest a nonnegligible contribution from metal centres. This is nicely consistent with the results of the theoretical analysis described below.

Attempts to demonstrate the presence of ferrocenium centres in salts such as **(1a)** [BF_4], **(2a)** [BF_4], **(1b)** [BF_4], **(2b)** [SbF_6] and related complexes by Mössbauer spectroscopy were not successful. The spectra of the salts showed essentially the pattern of the neutral precursors **(1a,b** and **2a,b)** with an isomer shift of $\delta \approx 0.51$ mm s^{-1} and a quadrupole splitting of $\Delta \approx 2.30$ mm s^{-1}, although small amounts of Fe(III) could be detected [22].

2.3. Theoretical study

Fig. 4 shows the structure of the compound [$Cp(PH_3)Rh\{(SC_5H_4)_2Fe\}$], which has been used as a model of the X-ray authenticated species [$Cp^*(PMe_3)$-$Rh\{(SC_5H_4)_2Fe\}$] **(1a)** [18].

A qualitative bonding scheme for such a model was obtained by applying the isolobal analogy [23]. The rather complex fragment $CpRh(PH_3)$ is isolobal with the simple fragment methylene, CH_2 [24], the frontier MOs of which consist of two formally half-occupied levels (a_1 and b_2 in the local C_{2v} symmetry), these are equivalent to two localised hybrids pointing towards the vertices of a tetrahedron. These two orbitals transforming as a' and a'' in $CpRh(PH_3)$ (its local symmetry is the same as that of the whole complex molecule, C_S), will be the fragment MOs responsible of the bonding interaction with the sulfur atoms in [$Cp(PH_3)Rh$-$\{(SC_5H_4)_2Fe\}$].

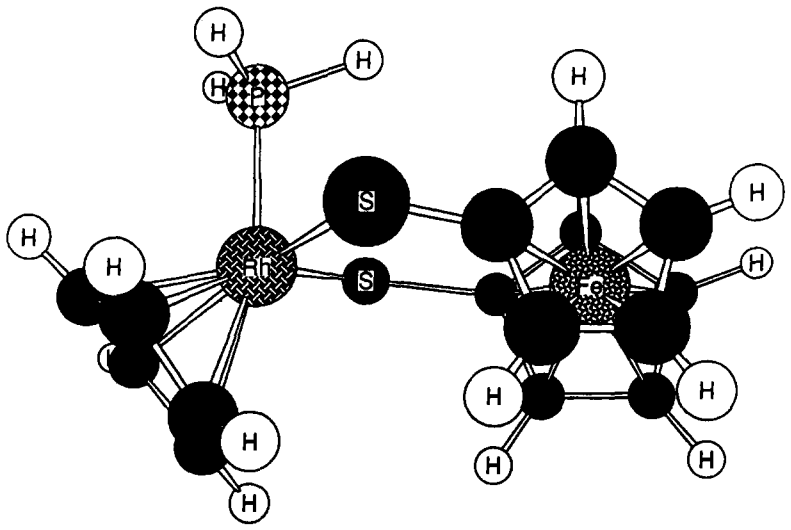

Fig. 4. Perspective view of the model compound [$Cp(PH_3)Rh\{(SC_5H_4)_2Fe\}$].

Even though such a qualitative picture is rather useful for understanding the main features of the bonding interaction between the two fragments $CpRh(PH_3)$ and $Fe(C_5H_4S)_2$, the quantitative description of the bonding scheme from the DV-Xα results is actually quite different.

Table 2 summarises the eigenvalues and the Mulliken [25] charge density analysis of the nineteen highest occupied and of the two lowest unoccupied MOs, as obtained by DV–Xα calculations. The analysis indicates that, despite the very low symmetry of the molecule, it is still possible to assign the t_{2g}- or the e_g-like designations to the Fe-localized MOs [26]. Unfortunately, this is partially prevented as far as the Rh atom is concerned [27]. Actually, only the MOs $26a'$ (mainly localised on the t_{2g}-like Rh $4d_{xz}$) and $28a'$ (with a significant contribution from the e_g-like Rh $4d_{z^2}$) are purely t_{2g}- or e_g-like in character. The high percentage localization of the Rh 4d AOs to MO $21a''$ (74%) is misleading; Actually, both the t_{2g}-like Rh $4d_{yz}$ (47%) and the e_g-like Rh $4d_{xy}$ (24%) contribute to this 74% [28]. The nature of the MOs $28a'$ and $24a'$, illustrated in Fig. 5, which represent the antibonding and bonding combinations of the occupied Rh $4d_{x^2-y^2}$ with one of the $C_5H_5^-$ π levels [28] is particularly interesting. The MOs $25a'$, $20a''$, $23a'$ and $18a''$ are simply the occupied π levels of the $C_5H_5^-$ rings bonded to the Fe atom.

Two further points deserve to be discussed, (i) the nature of the HOMO and (ii) the nature of the accidentally degenerate MOs $17a''$ and $21a''$.

The nature of the HOMO is particularly important because it is directly related to the oxidation processes observed in the electrochemical experiments. The HOMO $32a'$ is the in-phase linear combination of the S $3p_z$ AOs with a significant participation of the Rh 4d AOs. Certainly, $32a'$ is the MO involved in the first oxidation process and most probably in the second as well [29].

The accidentally degenerate levels $17a''$ and $21a'$ are responsible for the S–Rh σ interaction. Considering the qualitative electron count above, it might seem strange to find two, rather than one [31], highly *S*-localized MOs responsible for the Rh–S σ interaction. As a whole, one would expect to find four occupied MOs [three t_{2g}- ($4d_{xz}$, $4d_{yz}$, $4d_{x^2-y^2}$) and one e_g-like (d_{xy})] strongly localised on the Rh 4d AOs plus the n^+ combination of the *S* radical lobes. The presence of the n^- combination, in addition to the n^+ has to be traced back ultimately to the absence of an e_g-like MO mainly Rh $4d_{xy}$ in character among the occupied levels [32]. In the context it is noteworthy that the gross atomic charges

Table 2
SCM DV atomic character for $[(\eta^5\text{-}C_5H_5)Rh(PH_3)\{Fe(\eta^5\text{-}C_5H_4S)\}_2]$

MO	Eigenvalue ε (eV)	Population (%)										Character
		Rh			Fe			S	PH_3	(C_5H_5)	$(C_5H_4)_2$	
		s	p	d	s	p	d					
$33a'$	3.24	0	1	27	0	0	2	21	29	16	4	(Rh-P)σ [a]
$24a''$	3.44	0	0	16	0	0	25	15	0	22	22	(Rh-S)σ [a]
$32a'$ *	5.06	0	0	15	0	0	4	65	2	6	8	$3p_z$ S n^+
$23a''$	5.12	0	0	17	0	0	0	74	1	0	8	$3p_z$ S n^-
$31a'$	5.70	0	0	1	2	0	73	8	0	0	16	Fe 3d t_{2g}-like
$30a'$	5.85	1	0	4	0	0	56	19	1	5	14	Fe 3d t_{2g}-like
$22a''$	6.15	0	1	9	0	0	6	47	2	28	7	$3p_y$ S n^-
$29a'$	6.21	0	0	6	0	0	71	5	0	1	17	Fe 3d t_{2g}-like
$28a'$	6.43	0	0	39	0	0	19	7	2	18	15	($C_5H_5^-$-Rh 4d e_g-like) [b]
$27a'$	6.73	2	0	20	0	0	20	25	3	1	29	$3p_y$ S n^+
$26a'$	7.29	1	0	74	0	0	0	7	9	3	6	Rh t_{2g}-like (d_{xz})
$21a''$	7.50	0	0	71	0	0	1	15	6	4	3	Rh t_{2g}-like (d_{yz}) + e_g-like (d_{xy})
$25a'$	7.67	0	0	1	0	1	1	7	1	4	85	π-$C_5H_4^-$
$20a''$	8.00	0	0	1	0	0	23	3	0	0	73	π-$C_5H_4^- \rightarrow (d_{yz}, d_{xy})_{Fe}$
$24a'$	8.24	0	0	10	0	0	0	2	13	58	17	π-$C_5H_5^-$
$19a''$	8.63	0	0	24	0	0	9	4	0	38	25	π-$C_5H_5^- \rightarrow (d_{xy})_{Rh}$
$23a'$	8.74	0	0	3	0	0	0	18	3	7	69	π-$C_5H_4^-$
$18a''$	8.76	0	0	7	0	0	13	16	0	13	51	π-$C_5H_4^- \rightarrow (d_{yz})_{Fe}$
$22a'$	9.74	0	0	39	0	0	0	1	44	15	1	(Rh-P)σ
$17a''$	9.89	0	0	7	0	0	3	31	5	6	48	(Rh-S)σ
$21a'$	9.89	0	0	8	0	0	0	40	3	16	33	(Rh-S)σ

[a] Highest occupied MO.
[b] Antibonding orbital.

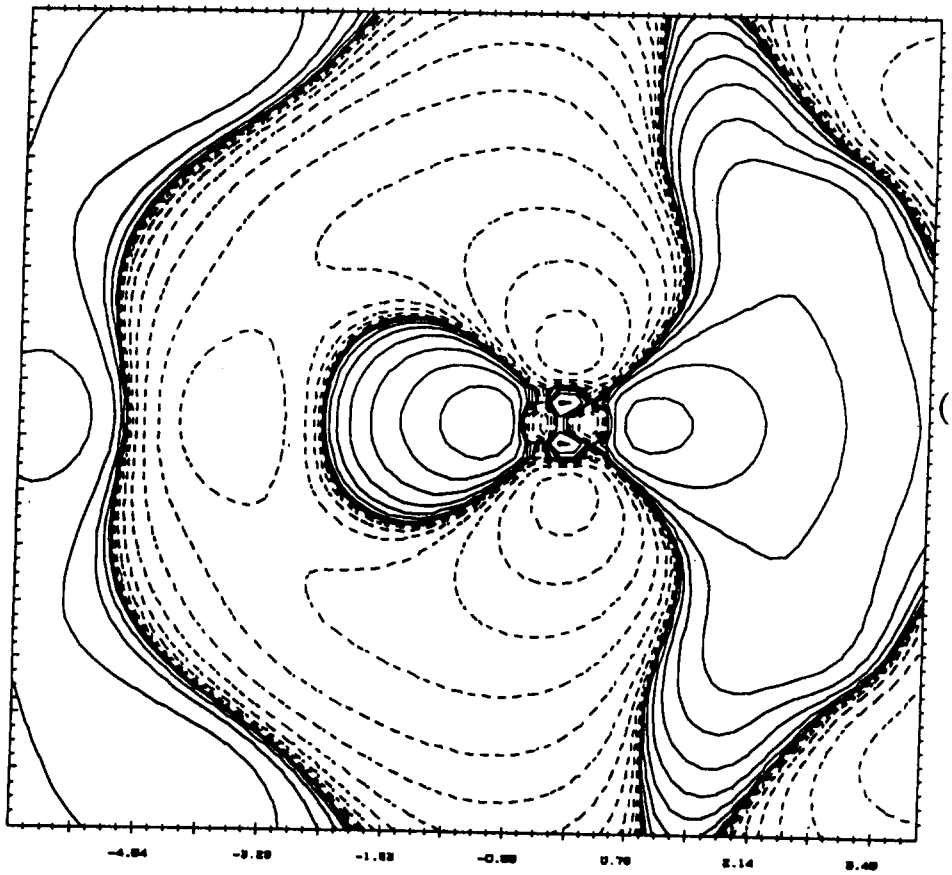
(a)

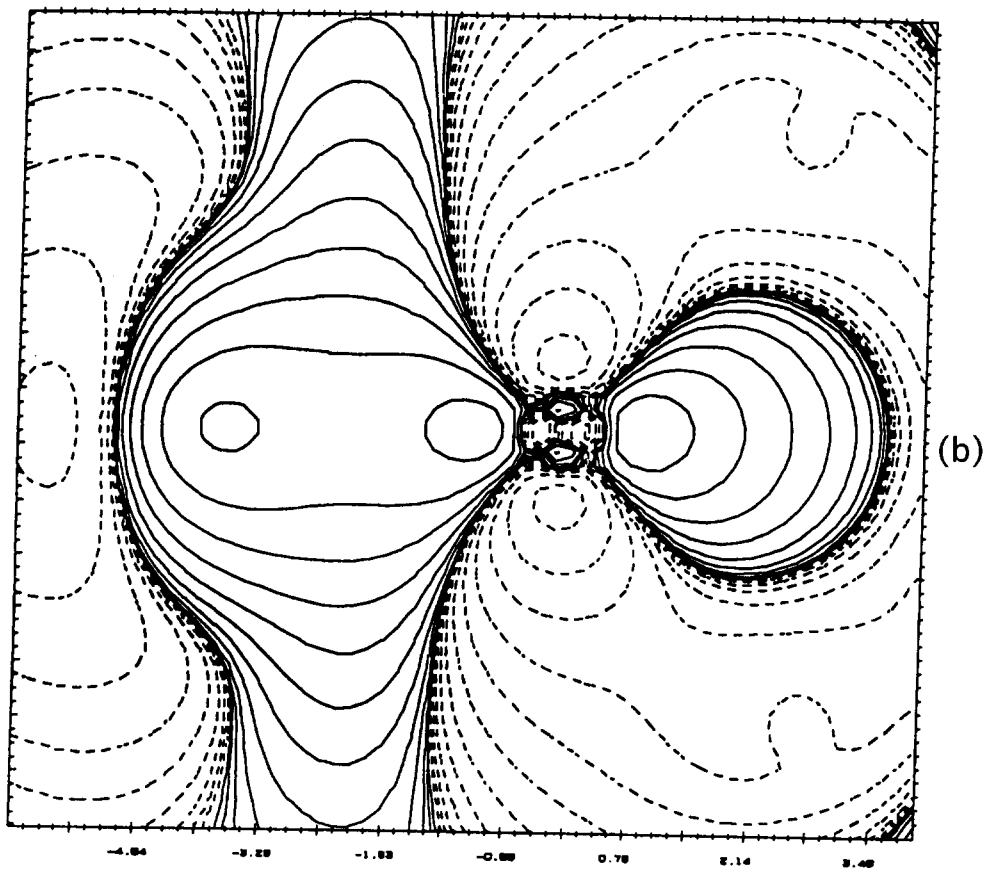
(b)

(Q) as well as the integrated charges [33] ($\int_Q$) of the Fe (formally in the II oxidation state) and the Rh (formally in the III oxidation state) atoms are quite similar (Q_{Fe} = 1.69 e, Q_{Rh} = 1.34 e; $\int Q_{Fe}$ = 0.77 e, $\int Q_{Rh}$ = 0.86 e), indicating extensive charge redistribution.

3. Conclusions

The heterodimetal complexes under study undergo two successive one-electron oxidation steps. In general, the abstraction of the first electron is reversible while the removal of a second electron leads to secondary processes which make it irreversible. In principle, both metals are able to lose an electron. From the EPR and a few preliminary Mössbauer data, it appears that the monocations generated by either chemical or electrochemical oxidation are not typical ferrocenium cations. The theoretical study carried out for a simplified model complex, $[Cp(PH_3)Rh\{(SC_5H_4)_2Fe\}]$, indicates that the HOMO is involved in Rh–S bonding. Initial oxidation at this part of the complex molecule is compatible with the results of the electrochemical study.

4. Experimental

4.1. Material and apparatus

Material and apparatus for electrochemistry have been described elsewhere [17]. All potential values are referred to the saturated calomel electrode (SCE). Under the present experimental conditions, the one-electron oxidation of ferrocene occurs at $E^{\alpha} = +0.45$ V.

4.2. Calculation details

The electronic structure of the model compound $[Cp(PH_3)Rh\{(SC_5H_4)_2Fe\}]$ has been investigated by performing first principle discrete variational DV-$X\alpha$ quantum mechanical calculations. The non-relativistic form of the one-electron Schrödinger equation can be written (in Hartree atomic units, σ represents spin) as

$$H_\sigma \Psi_{i\sigma}(\mathbf{r}) = \varepsilon_{i\sigma} \Psi_{i\sigma}(\mathbf{r}) \quad (1)$$

where

$$H_\sigma = \left[-\frac{1}{2}\nabla^2 + V_c(\mathbf{r}) + V_{xc,\sigma}(\mathbf{r}) \right] \quad (2)$$

The three terms refer to the kinetic energy, the Coulomb potential and the exchange-correlation potential, respectively. As far as the effective single particle exchange-correlation potential is concerned, the Slater $X\alpha$ form [30] (see Eq. (3)) has been employed. Throughout the calculations we used $\alpha = 0.7$, close to the Kohn–Sham value of 2/3. Variations of α between 2/3 and 0.7 have no significant effects on our results.

$$V_{xc,\sigma} = -3\alpha \left[\frac{3\rho_\sigma}{4\pi} \right]^{\frac{1}{3}} \quad (3)$$

The matrix elements of the effective Hamiltonian and of the symmetry orbital overlap matrix S are evaluated as discrete sums over a set of sample points. This set includes only pseudorandom diophantine points [34,35].

The occupation of each MO was determined by applying Fermi–Dirac statistics. The Coulomb potential was computed by one-dimensional integration by replacing the actual electron charge density with a model density, i.e. the "true" electron charge density was approximated by using a linear combination of basis functions, chosen in the present case to be the atomic radial densities. The coefficients of this expansion were fitted by a least-square procedure [35].

An extended basis set was used for Rh, Fe, S and P atoms (Rh 1s–5d AOs; Fe, 1s–4d AOs; S, 1s–3d AOs; P, 1s–3d AOs) while a minimal basis set was employed for C and H. Spherical wells (2 Ry deep) having an internal and external radius of 4.0 and 6.0 a.u., respectively, were added to the atomic potentials. Such a procedure provides a practical means for extending the basis to deal with diffuse orbitals. Moreover, it is flexible enough so that the basis sets can be optimized for the particular molecular application.

The experimental geometry of the modelled compound [18] was idealized to C_S symmetry. The calculations were performed on a DEC5200/CX (DIGITAL Equipment) work station at the Inorganic Chemistry Department of the University of Padova.

Acknowledgements

This work was partially supported by the Ministero dell'Università e della Ricerca Scientifica e Tecnologica (MURST, quota 60%) of Italy.

References and notes

[1] P.D. Beer, J.E. Nation, S.L.W. McWhinnie, M.E. Harman, M.B. Hursthouse, M.I. Ogden and A.H. White, *J. Chem. Soc., Dalton Trans.*, (1991) 2485, and references therein.

Fig. 5. DV-$X\alpha$ contour plots in the XY plane of the: (a) $28d'$ MO; (b) $24d'$ MO. Logarithmic contour levels are $\pm 8 \times 10^{-4}$; $\pm 16 \times 10^{-4}$; $\pm 32 \times 10^{-4} \ldots e^{1/2}/\text{Å}^{3/2}$.

[2] P. Zanello, in A. Togni and T. Hayashi (eds.), "*Ferrocenes. From Homogeneous Catalysis to Material Science*", VCH, Weinheim, 1995, Chap. 7.
[3] D.L. DuBois, C.W. Eigenbrot, Jr., A. Miedaner, J.C. Smart and R.C. Haltiwanger, *Organometallics, 5* (1986) 1405.
[4] D.A. Clemente, G. Pilloni, B. Corain, B. Longato and M. Tiripicchio-Camellini, *Inorg. Chim. Acta, 115* (1986) L9.
[5] B. Corain, B. Longato, G. Favero and D. Ajò, *Inorg. Chim. Acta, 157* (1989) 259.
[6] T.M. Miller, K.J. Ahmed and M.S. Wrighton, *Inorg. Chem., 28* (1989) 2347.
[7] P. Braunstein, L. Douce, F. Balegroune, D. Grandjean, D. Bayeul, Y. Dusausoy and P. Zanello, *New J. Chem., 16* (1992) 925.
[8] B. Longato, G. Pilloni, G. Valle and B. Corain, *Inorg. Chem., 27* (1988) 956.
[9] A.J. Arce, P.A. Bates, S.P. Best, R.J.H. Clark, A.J. Deeming, M.B. Hursthouse, R.C.S. McQueen and N.I. Powell, *J. Chem. Soc., Chem. Commun.*, (1988) 478.
[10] S. Colbran, B.H. Robinson and J. Simpson, *J. Chem. Soc., Chem. Commun.*, (1982) 1361.
[11] S. Colbran, B.H. Robinson and J. Simpson, *Organometallics, 2* (1983) 943.
[12] S. Colbarn, B.H. Robinson and J. Simpson, *Organometallics, 2* (1983) 952.
[13] B.H. Robinson, J. Simpson and M.E. Trounson, *Aust. J. Chem., 39* (1986) 1435.
[14] W.H. Watson, A. Nagl, S.H. Wang and M.G. Richmond, *J. Organomet. Chem., 445* (1993) 163.
[15] P. Zanello, *Struct. Bonding (Berlin), 79* (1992) 101.
[16] P. Diversi, S. Iacoponi, G. Ingrosso, F. Laschi, A. Lucherini, and P. Zanello, *J. Chem. Soc., Dalton Trans.*, (1993) 351.
[17] P. Zanello, G. Opromolla, M. Casarin, M. Herberhold and P. Leitner, *J. Organomet. Chem., 443* (1993) 199.
[18] M. Herberhold, G.-X. Jin, A.L. Rheingold and G.F. Sheats, *Z. Naturforsch., 47b* (1992) 1091.
[19] E.R. Brown and J.R. Sandifer, in B.W. Rossiter and J.F. Hamilton, (eds.), "*Physical Methods of Chemistry. Electrochemical Methods*, Vol. 2, Wiley, New York, 1986, Chap. 4.
[20] P. Zanello, in I. Bernal, (ed.), "Stereochemistry of Organometallic and Inorganic Compounds", Elsevier, Amsterdam, Vol. 4, 1990, pp. 181–366.
[21] D.M. Duggan and D.N. Hendrickson, *Inorg. Chem. 14* (1975) 955.
[22] J. Siver, personal communication, 1993–1994.
[23] (a) R. Hoffmann, *Angew. Chem., 94* (1982) 725; (b) idem, *Angew. Chem. Int. Ed. Engl., 21* (1982) 711.
[24] $C_5H_5^-$ is isolobal with $(CO)_3$, and the Lewis basicities of PH_3 and CO are comparable, being accounted for by the P and C lone pairs, respectively [23]. As a whole, $(C_5H_5)Rh(PH_3)$ is therefore isolobal with $M(CO)_4$ [$M = d^8$ metal atom, e.g. Fe] and both fragments are isolobal with CH_2.
[25] R.S. Mulliken, *J. Chem. Phys., 23* (1955) 1833.
[26] It has to be kept in mind that, since $C_5H_5^-$ is isolobal with $(CO)_3$, $(C_5H_5)_2^{2-}$ will be isolobal with $(CO)_6$ and, consequently, $Fe(C_5H_5)_2$ will remember its octahedral parentage. In this way, we can divide the five 3d-Fe AO's into two sets, three t_{2g}-like and two e_g-like. The former, which is completely occupied in $Fe(C_5H_5)_2$, is strongly localised on the metal atom and involved (even though to a different extent in the local D_{5d} symmetry of ferrocene) in back-donation into ligand virtual orbitals. The latter, which is completely unoccupied, accounts for the bonding interaction between the filled ligand-based π orbitals and the empty Fe-3d AOs.
[27] The local symmetry of the $CpRh(PH_3)$ fragment (C_S) is lower than that of the $Fe(SC_5H_4)_2$ fragment (C_{2v}) with the consequence that Rh t_{2g}- and e_g-like AOs are extensively mixed.
[28] The partner of MO $21a''$ is $19a''$, with a higher participation of $4d_{xy}$ (15%) than $4d_{yz}$ (9%). Incidentally, this level accounts for the donor interaction with $4d_{xy}$ of one of the occupied π levels, deriving from the degenerate e_1 set of the C_5H_5.
[29] A transition state [30] calculation relative to the HOMO $32a'$ has been run to take into account relaxation of the electronic structure upon ionization. No energy ordering inversion between the HOMO $32a'$ and the second HOMO $23a''$ was found.
[30] J.C. Slater, in "*Quantum Theory of Molecules and Solids. The Self-Consistent Field for Molecules and Solids*", Vol. 4, McGraw-Hill, New York, 1974.
[31] Qualitatively, one would expect two sulphur-localized radical lobes which should give rise to an in-phase (n^+) and an out-of-phase (n^-) linear combination, with the former being occupied and the latter being empty.
[32] The oxidation state of the Rh atom is assumed to be III.
[33] The integrated charge is the electronic charge found in the nearest volume surrounding each atom (f_Q). f_Q is particularly useful when extended basis sets are employed in order to achieve a detailed description of the metal-ligand covalent interactions.
[34] D.E. Ellis and G.S. Painter, *Phys. Rev. B, 2* (1970) 2887.
[35] B. Delley and D.E. Ellis, *J. Chem. Phys., 76* (1982) 1949.